Accepted Manuscript

Synergistic Effects of Spray-Coated Hybrid Carbon Nanoparticles for Enhanced Electrical and Thermal Surface Conductivity of CFRP Laminates

Yan Li, Han Zhang, Yi Liu, Huasheng Wang, Zhaohui Huang, Ton Peijs, Emiliano Bilotti

PII: S1359-835X(17)30399-8
DOI: https://doi.org/10.1016/j.compositesa.2017.10.032
Reference: JCOMA 4821

To appear in: *Composites: Part A*

Received Date: 20 June 2017
Revised Date: 25 October 2017
Accepted Date: 30 October 2017

Please cite this article as: Li, Y., Zhang, H., Liu, Y., Wang, H., Huang, Z., Peijs, T., Bilotti, E., Synergistic Effects of Spray-Coated Hybrid Carbon Nanoparticles for Enhanced Electrical and Thermal Surface Conductivity of CFRP Laminates, *Composites: Part A* (2017), doi: https://doi.org/10.1016/j.compositesa.2017.10.032

Synergistic Effects of Spray-Coated Hybrid Carbon Nanoparticles for Enhanced Electrical and Thermal Surface Conductivity of CFRP Laminates

Yan Li[1,2], Han Zhang[1,3], Yi Liu[1], Huasheng Wang[1], Zhaohui Huang[4], Ton Peijs[1,3*], Emiliano Bilotti[1,3*]

[1] School of Engineering and Materials Science, and Materials Research Institute, Queen Mary University of London, Mile End Road, E1 4NS, London, UK

[2] Gemmological Institute, China University of Geosciences, Wuhan, 430074, P. R. China.

[3] Nanoforce Technology Ltd., Joseph Priestley Building, Mile End Road, E1 4NS London, UK

[4] School of Materials Science and Technology, China University of Geosciences, Beijing, 100083, P. R. China.

Corresponding authors: e.bilotti@qmul.ac.uk; t.peijs@qmul.ac.uk

Keywords: *Graphene, Carbon fibres, Nanocomposites, Electrical properties, Thermal properties, Lightning strike protection*

ABSTRACT

Carbon fibre reinforced plastics (CFRPs) are intensively used in modern aircraft structures because of their superb specific mechanical properties. Unfortunately their electrical and thermal conductivities are not sufficiently high for some applications like electromagnetic interference (EMI) shielding and lighting strike protection (LSP). The addition of external metallic structures, such as aluminium or copper mesh, is generally required, with a compromise in terms of increased mass and manufacturing cost as well as reduced corrosion resistance. In the present work spray coating of carbon nanoparticles was utilised as a simple method to locally increase the electrical and thermal suface conductivity of CFRPs. The combined use of carbon nanotubes (CNTs) and graphene nanoplatelets (GNPs) synergistically reduced the CFRPs surface resistivity by four orders of magnitude (from 2-3 Ω/sq to 3×10^{-4} Ω/sq) and increased the thermal conductivity by more than 7 times (from 200 $W\cdot m^{-1}\cdot K^{-1}$ to 1500 $W\cdot m^{-1}\cdot K^{-1}$), opening up possibilities for the replacement of metallic mesh structures for EMI shielding and LSP. An analytical model was introduced based on a one-dimensional heat conduction approach to predict the effective thermal conductivity for the hybrid nanofiller coating layer and its findings showed good agreement with experimental data.

1. INTRODUCTION

Carbon fibre reinforced plastics (CFRPs) have been increasingly used for modern aircraft structures and wind turbines because of their excellent in-plane mechanical properties (stiffness and strength) and lightness [1-3]. However, unlike their metallic counterparts, CFRP structures do not readily conduct away the extremely high electrical current and electromagnetic force generated by a lightning strike [4]. CFRPs have a relatively low electrical conductivity (σ), particularly in the out-of-plane direction [5] (e.g., $\sigma_{out\text{-}of\text{-}plane}$ =3.2×10^{-3} S·m^{-1} for unidirectional CFRPs with V_f = 60%) [6]) and need to be engineered for lightning strike protection (LSP) to withstand a lightning tolerance comparable to metallic structures. The principle of LSP is to offer a safe conductive path on the exterior skin of a composite panel. In an ideal case most of the lightning current will remain located at the highly conductive skin of the aircraft and will quickly exit off the aircraft without fatal damages. Current LSP solutions used in commercial aircraft composite structures are based on meshes or foils made of highly conducting metals and alloys. These meshes can be comprised of aluminium (Al), copper (Cu) or bronze (CuSn) wire, and can either be co-woven or commingled with the carbon fibre in a prepreg or fabric ply, or bonded separately as a mesh to the outermost laminate layer [7, 8]. However, in the case of aluminium mesh, galvanic corrosion can occur if moisture penetrates the composite's exterior skin [9]. Galvanic action can be particularly severe for metals with low electrode potentials. Aluminium presents a greater risk of galvanic corrosion than most other metallic materials. Copper mesh eliminates the galvanic reaction risk, but weighs at least twice as much as aluminium [10]. General drawbacks of using metal meshes are the added mass of structural elements (e.g. typical areal densities of metallic foil are up to 1,600 g·m^{-2} [10]), added manufacturing cost, as well as reduced corrosion resistance and durability [9, 11]. It should also be mentioned that solutions based on impregnation of metallic meshes and foils reduce the extent of damage as a result of lightning strike, but do not eliminate the problem. Thus, new solutions that allow for an increased resistance to atmospheric discharges, while at the same time simplifying the manufacturing process are highly desirable. One recent approach is the use of conductive nanofillers, in particular carbon nanofillers like carbon nanotubes (CNTs), graphene and graphene nanoplatelets (GNPs). CNTs and graphene have attracted significant attention due

to their intrinsically high mechanical properties (E_{CNT} = 1 TPa [12], $E_{graphene}$ = 1 TPa [13]), thermal conductivity (λ_{CNT} = 2000-3000 $W \cdot m^{-1} \cdot K^{-1}$ [14], $\lambda_{graphene}$ = 5000 $W \cdot m^{-1} \cdot K^{-1}$ [15]) and electrical conductivity (σ_{CNT} = 3.3×10^6 $S \cdot m^{-1}$ [16], $\sigma_{graphene}$ = 10^8 $S \cdot m^{-1}$ [16, 17], also high charge mobility, v_{CNT} = 10^5 $cm^2 \cdot V^{-1} \cdot s^{-1}$ [18], $v_{graphene}$ = 2×10^5 $cm^2 \cdot V^{-1} \cdot s^{-1}$ [19]), combined with their large aspect ratio (AR_{CNT} = 500-10^4 [20], $AR_{graphene}$ = 500-2000 [21, 22]). Unfortunately the electrical conductivities of GNP/epoxy (σ_{max} = 1 $S \cdot m^{-1}$ at 2.5 vol.% GNP [14]) and CNT/epoxy (σ_{max} = 10^4 $S \cdot m^{-1}$ at 7.5 wt.% CNT) composites are still relatively low. Substantially increasing the nanofiller content is not a viable route as other problems like high resin viscosity, mechanical property reduction due to agglomeration and nanoparticle filtration during infusion will arise [23]. The use of hybrid nanofillers, like combinations of multi-wall carbon nanotubes (MWCNTs) and carbon black [24-28], have been reported to lead to synergistic effects. An interesting alternative approach has been the use of buckypaper in CFRPs [29]. Wang *et al.* [30] successfully impregnated single wall carbon nanotube (SWCNT) buckypaper with resin for improved LSP. Drzal *et al*. [17] reported that the surface electrical resistance of GNP/CFRP composite (GNP paper inserted into CFRP laminate: σ = 2.2×10^5 $S \cdot m^{-1}$) was ca. 3×10^{-4} Ω·m. Gou *et al.* [31] showed a positive correlation between electrical conductivity of the surface coating and damage from lightning strike and employed a specialty paper made of carbon nanofibres and Nickel (Ni) nanostrands as a surface layer (ca. 1×10^{-4} Ω·m) on CFRP panels as potential replacement materials for LSP. Although promising results have been reported, buckypapers and other hybrid nanoparticle papers are difficult to implement in an industrial environment and scaled up to the size required for practical engineering applications.

Another recent approach for LSP is based on the use of intrinsically conductive polymers (ICPs). ICPs are possible alternatives for enhancing the electrical properties of CFRP, while the mass of the resulting composite structure remains mostly unaffected. Doped polyaniline (PANI) and its derivatives are the most widely studied ICPs in such composites [32-37]. PANI has great potential in terms of its widespread commercial usability because of its high conductivity, easy synthesis, low cost, good environmental stability and availability. Yokozeki and Hirano [34, 38] investigated the development of CFRP using a PANI-based electrically conductive thermoset matrix with dodecylbenzenesulfonic acid (DBSA) and *p*-toluenesulfonic acid (PTSA) as dopants and divinylvenzene (DVB) as the crosslinking polymer to enhance its electrical properties in the through

thickness direction (0.74 S/cm). PANI polymer systems exhibit high conductivity, suitable viscosity for the fabrication of CFRPs, and sufficient toughness. These properties seem ideal for enhancing the electrical properties and LSP of CFRP [38]. However, it is worth noting that the thermal conductivity of PANI is less than 0.7 $W \cdot m^{-1}K^{-1}$, while its inferior stability also limits its applications. Therefore, it is of great interest to find alternative solutions to increase the electrical and thermal conductivities of CFRPs, especially for systems based on common epoxy resins.

Direct deposition of nanoparticles onto carbon fibre (CF) preforms can locally enhance both the surface electrical and thermal conductivities of CFRP, meanwhile overcoming the limitation of scalability. Spray coating, for instance, has been demonstrated to be a facile method to deliver CNTs and GNPs into CFRPs in a controlled and scalable manner [2, 39-41]. Chakravarthi *et al*. [42] obtained improved electrical conductivity of CFRPs by spray coating hybrid Ni-SWCNT on CF fabrics. Addition of 4 wt.% Ni-SWCNTs (0.2-0.4 Ω/sq) reduced the electrical resistivity of the reference laminate (10^9 Ω·m) by 10 orders of magnitude. The use of Ni, however, re-introduces the problem of galvanic corrosion. In the present work we will explore the possibility of an all-carbon based solution, in particular the exploitation of potential synergisms between CNT and GNP nanofillers, directly spray-coated onto CF preforms. CNTs have already been shown to align on GNP flakes, creating an inter-connected strong mixed nanofiller network. Shin *et al.* [43] reported synergistic toughening of composite fibres by self-alignment of reduced graphene oxide (GO) and CNTs. Yang *et al*. [44] improved mechanical and thermal properties of epoxy with hybrids of multi-layered GNPs and MWCNTs. The present work aims at enhancing the surface electrical and thermal conductivities of CFRP laminates using hybrid carbon nanofillers, deposited with a method which can be readily and cheaply implemented in the industrial scale manufacturing of CFRPs.

2. EXPERIMENTAL

2.1. Materials

Non-functionalised medium aspect ratio (>150) MWCNTs used in this work were produced by a chemical vapour deposition (CVD) process and were purchased from Cheap Tubes Inc. (US). GNPs,

1-2 µm in length and 2 nm in thickness, of relatively high aspect ratio (~600), were in-house produced by a liquid phase exfoliation process using probe sonication of natural graphite in N-Methyl-2-pyrrolidone (NMP) [45]. High speed centrifugation was utilized to control the size of the graphene and to warrant the quality of the GNPs.

The epoxy resin (EP) was an aeronautical grade epoxy (MVR444), based on a resin (MVR444R) and hardener (MVR444H), kindly supplied by Cytec Ltd. (UK). The density of the cured epoxy system was around 1.1 g/cm^3. The composite system employed consisted of woven carbon fibre fabric with a 4x1 Harness-Satin 5 (5HS) structure. Carbon fibre fabric/neat epoxy laminates were manufactured as baseline material. The mould release agent (Product No. 700-NC) was from Frekote, and an adhesive spray was purchased from 3M (Product No.: 10003901). The epoxy adhesive films used for encapsulating the nanoparticles after spraying was supplied by 3M™ (AF 130-2). Kapton® polyimide films (No.536-3952, thickness 50 µm) were purchased from RS Components Ltd. (UK).

2.2. Spray Coating

Nanoparticles were sprayed using an airbrush system from Iwata Performance (H4001 HP-CPLUS), connected with an Iwata air compressor. Probe sonication (Sonics, Model GEX 750, 20 kHz, 5000 J energy, 20 % amplitude) was used to disperse the nanofillers in acetone. A detailed illustration can be found in [2]. A heating stage with a controlled temperature of 80 °C was positioned underneath the fabrics during the spray coating process to facilitate the evaporation of the solvent. The nanofiller concentrations in acetone were 5 mg /150 ml and 10 mg/100 ml for CNTs and GNPs, respectively. Spray coated fabrics were encapsulated by a B-staged epoxy adhesive film, which was co-cured together with the epoxy resins during the curing process. The main aim of this film encapsulation was to avoid any release of airborne nanoparticles during subsequent handling and manufacturing, enhancing the feasibility of transfering this technology to an industrial environment (**Fig. 1**).

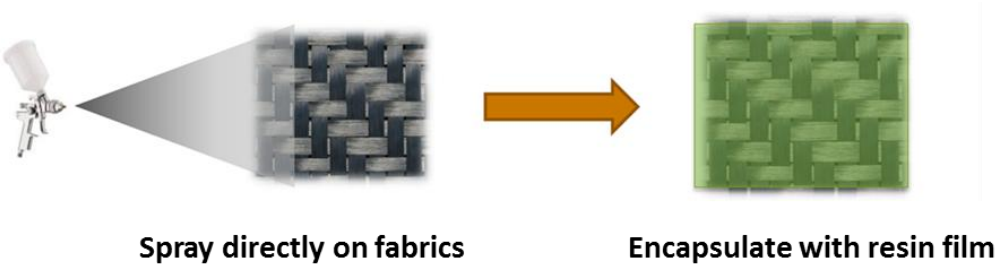

Fig. 1. Schematic illustration of spray coating of nanocarbons directly on carbon fibre fabrics folowed by encapsulation of the carbon nanofillers using an epoxy resin film.

Clearly, the CNT:GNP ratio is an important factor in optimizing such hybrid nanofiller systems [44]. Four formulations were investigated in the present work: 1) 50 mg CNTs, 2) 70 mg CNTs, 3) 60 mg CNTs + 10 mg GNPs, and 4) a reference sample sprayed with pure acetone (no nanoparticles). Note that the mass refers to the total mass of nanoparticles sprayed onto each of the two sides of a carbon fibre fabric of size 40 cm x 40 cm. The effectiveness of the sprayed nanomaterials onto the CF fabrics was considered with reference to a control sprayed onto an insulator substrate, while the spray rate and spraying efficiency was checked. CNT/acetone (50 mg CNTs) and CNT/GNP/acetone (60 mg CNTs + 10 mg GNPs) suspensions were prepared and spray coated on polyimide films (40 cm × 40 cm). Three experiments for each system have been performed. The spray rate was estimated from the ratio of the GNPs left on the film to the total amount of GNPs added in the suspension. The average spray rate is ca. 95 % (see **Table 1**). Different amounts of nanofiller suspension have been spray coated on the same insulating substrate with the thickness adjusted to control the bulk resistivity of the nanocoating layer.

Table 1. The spray rate and efficiency for spray coating.

Substrates (cm^2)	$M_{substrate}$ (M_1, g)	$M_{after\ coating}$ (M_2, g)	$\Delta M = M_2 - M_1$, (ΔM, g)	$M_{spray\ coating}$ (M, g)	Spray rate $\Delta M/M$
40 × 40	20.505	20.553	0.048	0.05	96.0%
		20.551	0.046	0.05	92.0%
		20.552	0.047	0.05	94.0%
40 × 40	20.505	20.574	0.069	0.07	98.5%
		20.573	0.068	0.07	97.1%
		20.570	0.065	0.07	92.8%
Average					95.1%

2.3. Fabrication of CFRP Laminates

CFRP panels (40 cm x 40 cm) were manufactured by vacuum assisted resin infusion (VARI). Dry carbon fibre fabric stacks consisted of one ply of CF fabric coated with nanoparticles on top of nine plies of woven CF fabrics without nanoparticles. All ten plies of fabric were laid up on a flat steel mould in the same direction and covered by a peel ply and flow media within the flexible bag for VARI. A detailed illustration can be found in [46, 47]. Epoxy resin was heated to 70 °C under vacuum for 20-30 min to reduce its viscosity and facilitate degassing. After degassing the hardener (@ 80 °C and magnetic stirring for 10 min) was added to the resin and the mixture was stirred for another 15 min. The mixing ratio of resin and hardener before curing is 10.0:5.8 w/w. A final degassing step was then performed for 30 min, followed immediately by infusion of the mixture into the preheated (90 °C) mould. After the completion of mould filling, the cure cycle involved; i) ramping to 120 °C (@ 3 °C·min^{-1}) followed by a 90 min isotherm, ii) ramping from 120 to 180 °C (@ 3 °C·min^{-1}) followed by a 180 min isotherm and iii) cooling down from 180 °C to room temperature (@ 3 °C·min^{-1}). Specimens were cut into test specimen with desired dimensions using a diamond cutting wheel. No visible defects and dry-spots were observed. The same procedures and parameters were applied for all neat resin reference specimens to highlight the effect of nano-modification. Weight fractions were estimated from the measured masses of the various constituents as they were added. Volume fractions were derived using the densities given in the experimental sections, assuming that voids and resin flash are both negligible. The thickness of the cured panels was 4.85-4.88 mm with a fibre volume fraction of around 50 %.

2.4. Characterisation Techniques

Morphological analysis

A morphological study was carried out using scanning electron microscopy (SEM) (FEI, Inspector-F, Netherlands) with an acceleration voltage of 20 kV. The morphology of the cured CFRP laminates after gold coating was investigated by imaging fracture surfaces. Transmission electron microscopy (TEM) (JEOL JEM-2010, Japan) was used to examine the morphology of the exfoliated graphene. Atomic force microscopy (AFM) (NT-MDT NTegra, Russia) was also used to study the morphology

of the graphene flakes. The AFM samples were prepared by drop casting a diluted GNP/acetone dispersion on a mica substrate. After evaporation of acetone, the specimens were scanned as prepared. Please refer to our previous publication for more detailed information [48].

Raman spectroscopy (Thermo Fisher Scientific Nicolet Almega XR, High-Performance Dispersive Raman Spectrometer, UK) was utilized to characterize of exfoliated GNP. Raman measurements were performed with a wavelength of 532 nm [48].

Electrical tests

Surface electrical resistance was measured by a two-probes method using a picoammeter (Keithley 6485, Textronix, US) and a DC voltage source (Agilet 6614C, US). Surface resistance tests were performed in accordance with ASTM D4496 – 87 standard [49]. The surface resistivity ρ_s in Ω/sq was calculated as below,

$$\rho_s = R_s(W / L) \qquad \text{Equation (1)}$$

where R_s is the surface resistance, *W* and *L* are the width and length of the specimen between electrodes, respectively.

Panels were cut into test specimen of 10 mm x 30 mm and silver paste was applied to the edges of the specimen ends to ensure good contact between the electrodes and the sample. To eliminate the effect of excess resin on the surface of the specimens, the surface electrical resistance was tested after up to 10 cycles of manual abrasion by sandpaper (Grade 1200). SEM was utilised to measure the thickness reduction of the specimens after each abrasion cycle.

Thermal tests

Thermocouples were used to measure the surface temperature of the composite specimens (50 mm x 70 mm) at different locations along the panel length. The variation in specimen surface temperature was measured upon heating the panel from one side by a heated metal strip with a constant temperature of 150 °C. Picolog software was used to record the temperature variation with time in this transient surface heat conduction test. A thermal imaging camera (FLIR system,

Model: FLIR A 35, UK) was used to take thermal images and videos of the temperature distribution along the panel while heating the panel from one side.

3. RESULTS AND DISCUSSION

3.1. Morphological Analysis

Natural graphite (NG) flakes exhibited lateral dimensions varying between 600 ± 150 µm and 800 ± 200 µm and thicknesses of ~40 µm (**Fig. 2a-b**), giving the initial NG flakes an apect ratio (AR) of 20 ± 5. After exfoliation via probe sonication in N-Methyl-2-pyrrolidone (NMP) solvent, the average length of the exfoliated graphene or few layer graphene (FLG) was around 1.23 ± 0.45 µm (**Fig. 2c-d**), while the thickness was ~2 nm (AR ≈ 600). The edges of the graphene sheets (**Fig. 2e-f**) indicated that single and few layer graphene were obtained without aggregation after liquid phase exfoliation. AFM images and Raman data (**Fig. 2g-h**) confirmed that FLG was obtained. Moreover, Raman spectra (**Fig. 2h**) of FLG (containing D, G and 2D peaks) confirmed a graphitic structure with low defect content.

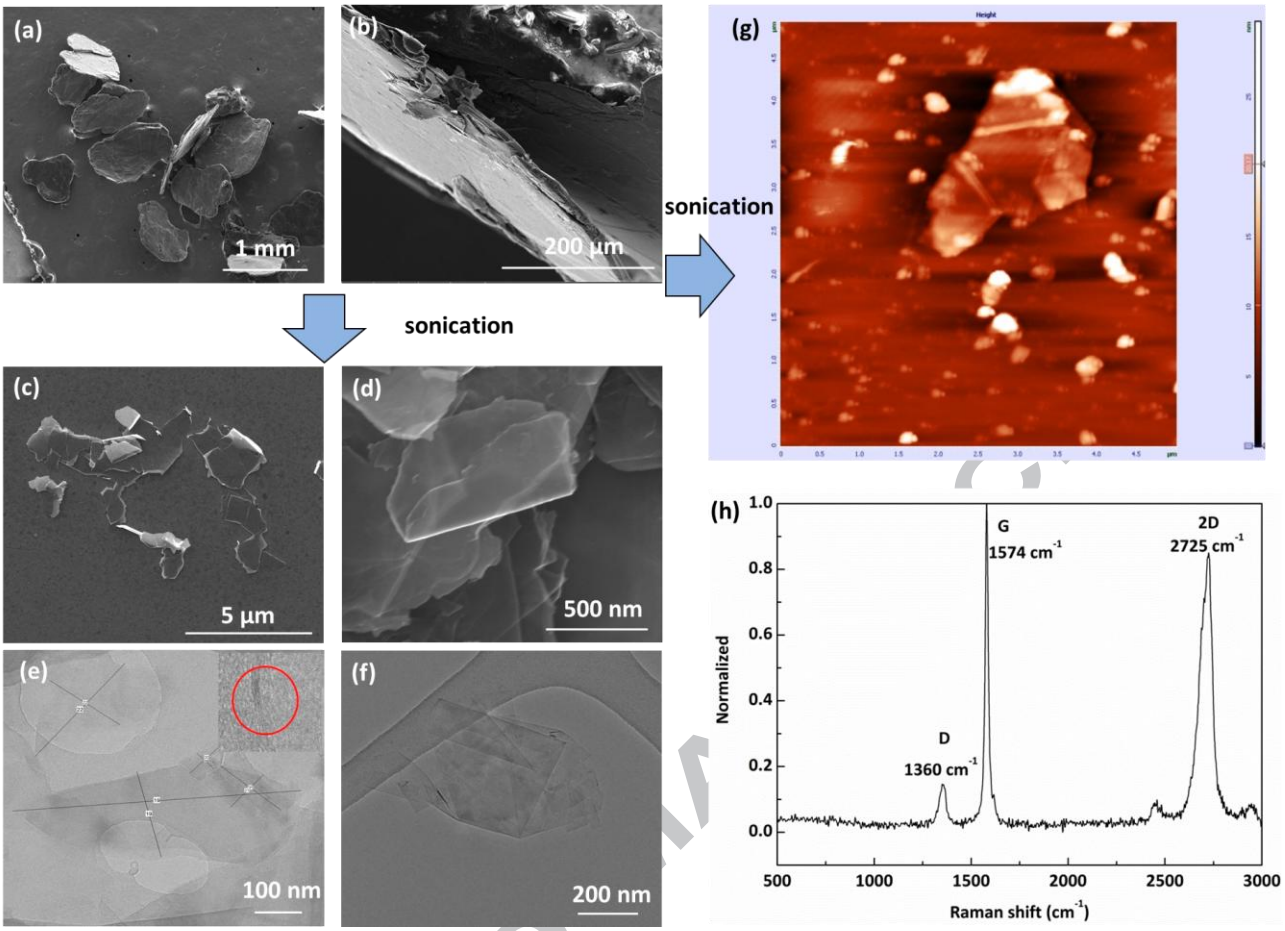

Fig. 2. (a-b) SEM images of natural graphite; representative (c-d) SEM, (e-f) TEM and (e) AFM images of exfoliated FLG obtained by probe sonication of NG in NMP solvent; (f) Raman spectra of FLG (containing D, G and 2D peaks) extracted from NMP solution, confirming a graphitic structure with low defect content.

Fig. 3a-c show the distribution of CNTs and CNT/GNP hybrids on carbon fibre fabrics after spray coating compared to reference CF without nanoparticles (**Fig. 3d**). CNTs are evenly distributed on the CF surface as interconnected small bundles or individual nanotubes (**Fig. 3a-b**). GNPs show the typical platelet type morphology (**Fig. 3c**). In the case of hybrid nanofillers the presence of GNPs does not appear to significantly modify the distribution of CNTs **(Fig. 3c-d).** CNT particles as "tiny dots" and flat GNPs (of 1-2 µm) can be identified from the CFRP cross-sections (**Fig. 3e-f**) and **Fig. 3g**, respectively, compared to the CFRP reference laminate (**Fig. 3h**).

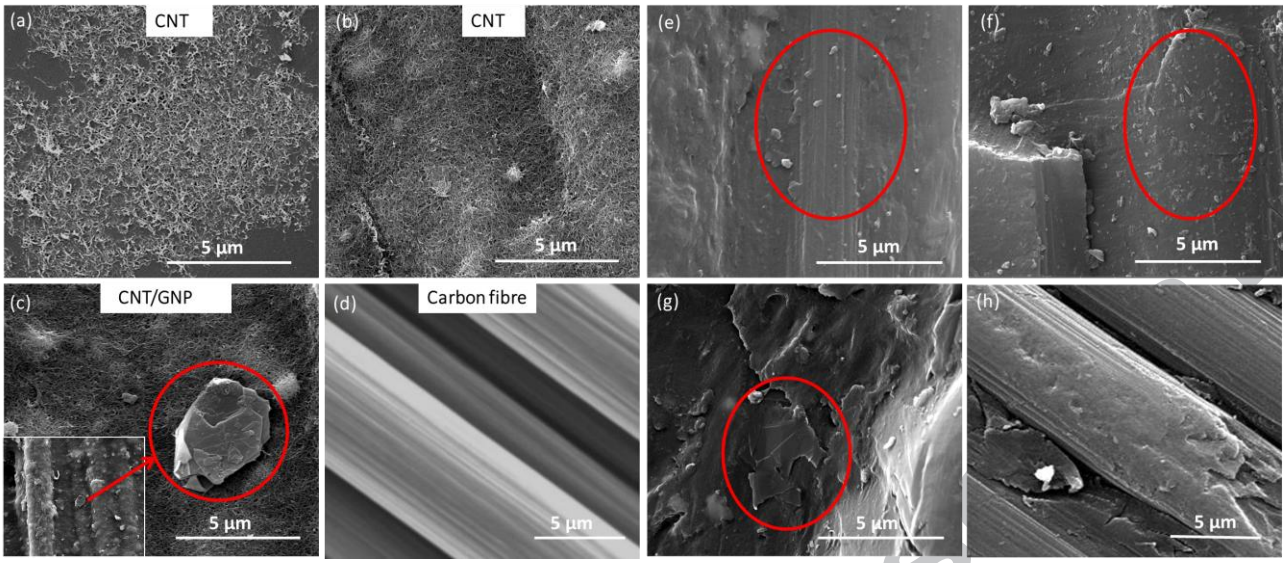

Fig. 3. SEM images of different amounts of nanoparticles sprayed on CF fabrics: a) 50 mg CNTs, b) 70 mg CNTs, c) 60 mg CNTs + 10 mg GNPs, d) reference sample without nanoparticles. SEM images of CFRP containing different amounts of nanoparticles: e) 50 mg CNTs, f) 70 mg CNTs, g) 60 mg CNTs + 10 mg GNPs, h) reference sample without nanoparticles.

3.2. Surface Electrical Resistivity

A synergistic effect between the two-dimensional (2D) GNPs and one-dimensional (1D) CNTs on electrical conductivity was found in the conductive coating layer. In addition, high electrical conductivity of graphene in the basal plane enhances the synergistic effect in terms of electrical conductivity. The electrical conductivity of the coating layer depends on the conductive percolated network, the weight ratio of GNPs to CNTs, and on the morphology of the layer [50].

The surface electrical resistivity of CFRP panels is plotted in **Fig. 4a.** A lower electrical resistivity is obtained with increasing amount of CNTs. An even lower electrical resistivity is observed when CNTs and GNPs are jointly used, which cannot be explained by a simple mixing rule, hence showing some synergistic effects, in analogy with a previous investigation [51]. By combining 1D nanoparticles like CNTs with 2D nanoparticle like GNPs one can envisage the formation of a more intricate 3D conductive network. Long and tortuous CNTs can bridge adjacent GNPs and, by this, inhibit their aggregation, resulting in a larger specific surface area and more conductive pathways [43, 52]. **Fig. 4a** also shows that the surface electrical resistivity of CFRP panels noticeably decreases as the external surface gets progressively removed by abrasion (increasing depth). The surface resistivity of the reference sample (without nanoparticles) decreases from 0.60 Ω/sq (@ 30 µm depth) to 0.01 Ω/sq (@ 180 µm depth) until it reaches a plateau in correspondence to a depth of 180 µm. For all samples containing nanoparticles, instead, the surface electrical resistivity

assumes a minimum at a depth of 180 µm, after which it increases, reaching the same plateau level as found in the reference samples. To explain this phenomenon, SEM micrographs of the sample's cross-sectional area were taken after each abrasion cycle (**Fig. 4f-i**). Initially the external surface of each sample shows an epoxy region, about 180 µm thick. With increasing number of abrasion cycles the epoxy region decreases in thickness (averaging ca. 30 µm/cycle), until the CF ply level is reached after about six abrasion cycles. Only for the samples containing spray coated nanoparticles, a new discrete region is found, just above the CF ply, in correspondence to a depth of 180 µm (after about six abrasion cycles). As shown in **Fig. 4c-e**, this new region is characterised by a highly dense nanoparticle layer, lying on top of the CF fabric layer (**Fig. 4c-e**). **Fig. 4b** shows a schematic of the cross-section of the samples, in the proximity of the external surface, constituted by up to three regions: (1) an epoxy insulating layer ($t \approx 180$ µm), (2) a nanoparticle modified layer ($t < 4\text{-}5$ µm) (not present in reference samples) and (3) the carbon fibre/epoxy laminate ($t \approx 50$ µm). This schematic, supported by the SEM micrographs in **Fig. 4f-i**, well explains the surface electrical resistivity data shown in **Fig. 4a**.

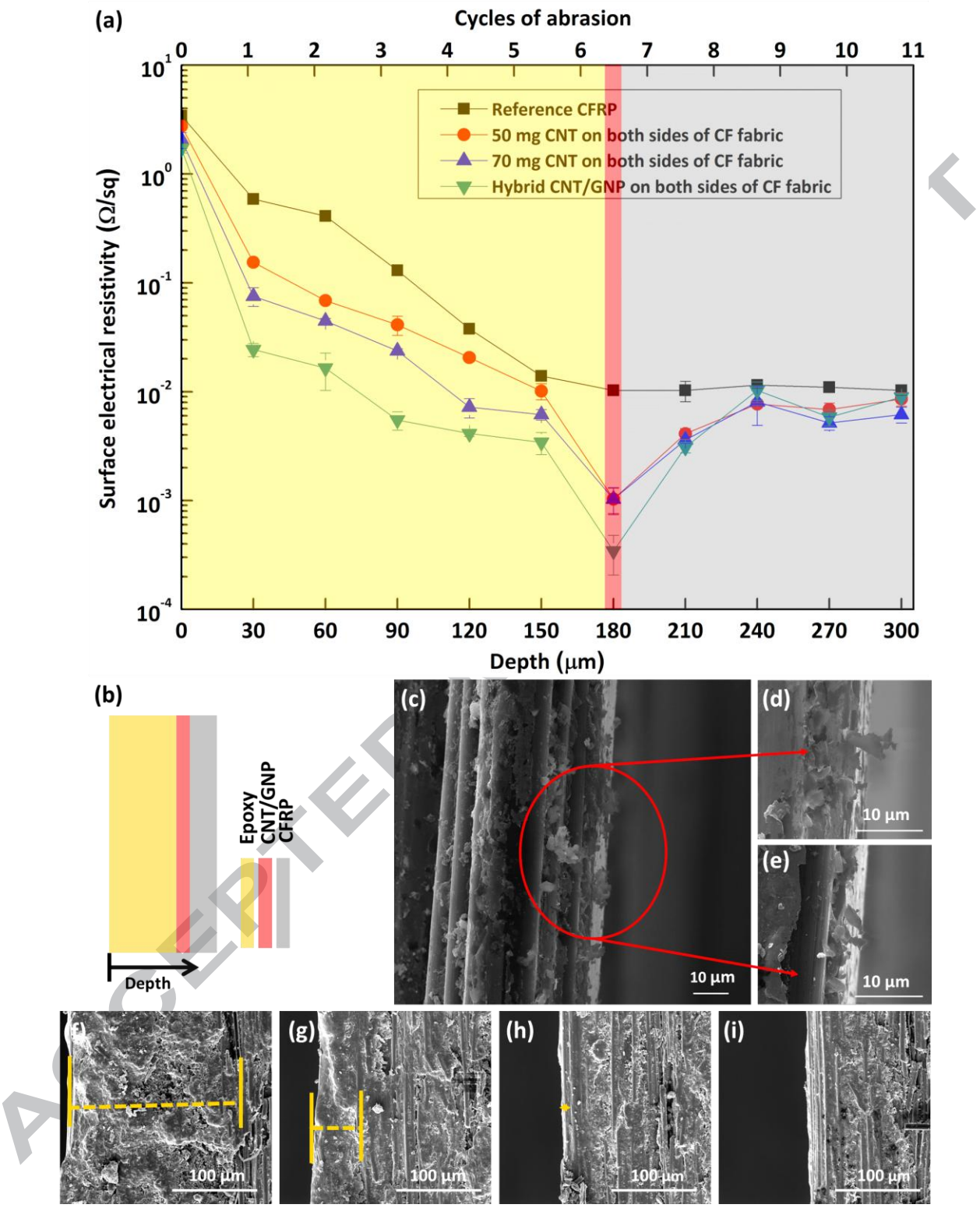

Fig. 4. (a) Surface electrical resisivity of different nanofiller modified CFRPs in relation to surface depth, (b) schematic of different surface layers of nanofiller modified CFRPs, (c-e) the exposure of GNP, (f-i) reduction in depth of matrix layer after 1st, 5th, 6th and 7th cycles of abrasion.

Our lowest value of electrical resistivity was 3.4×10^{-4} Ω/sq, and was obtained when the CFRP top ply was coated with CNT/GNP hybrids, which is comparable to the highest values found in scientific literature but at a lower overall nanofiller content (areal density ρ = 0.4 g·m^{-2}). Asmatulu *et al*. [9] for example obtained a resistivity of 1.9×10^{-4} Ω/sq by surface spray coating 8 wt.% GNP on carbon fibre, while Leng *et al.* [53] reached a value of 1.2×10^{-4} Ω/sq by inserting CNT based buckypaper. In addition, our surface electrical resistivity approaches the values of commercial Cu and Al meshes (0.79-1.26×10^{-4} Ω/sq [54], depending on the knit and solder structure of the metal wire mesh [53, 55]) but at a fraction of the areal density. Typical areal density values of commercial metal meshes range from 50 to 1000 g·m^{-2} [42-44], while the areal density of our CNT/GNP hybrid coating is as little as 0.4 g·m^{-2}. This offers great benefits in terms of weight savings and corrosion resistance, while the simplicity of the spray-coating deposition method overcomes problems of scalability and manufacturing costs.

During lighting strike it is expected that the heat generated will burn away the resin rich surface layer of the composite panel. It is expected that the presence of either a Cu or Al mesh or a GNP/CNT hybrid coating can then dissipate this large amount of energy quickly, hence minimizing the damage created by local heating during the event. However, it is expected that in most cases components after lightning strike would still require repairing or replacement.

3.3. Surface Heat Transfer and Theoretical Modeling

To evaluate the effect of the carbon nanofillers on heat transfer, different panels were subjected to a transient surface heat conduction test (inset **Fig. 5**). **Fig. 5** shows the evolution of the temperature with time at one end of the sample (position 2), while the temperature at the other end (position 1) is maintained at 150 °C. It is seen that the temperature at position 2 of panels coated with CNT/GNP hybrids is always higher than that of reference panels without nanocarbons, indicating a faster surface heat transfer through the coating layer.

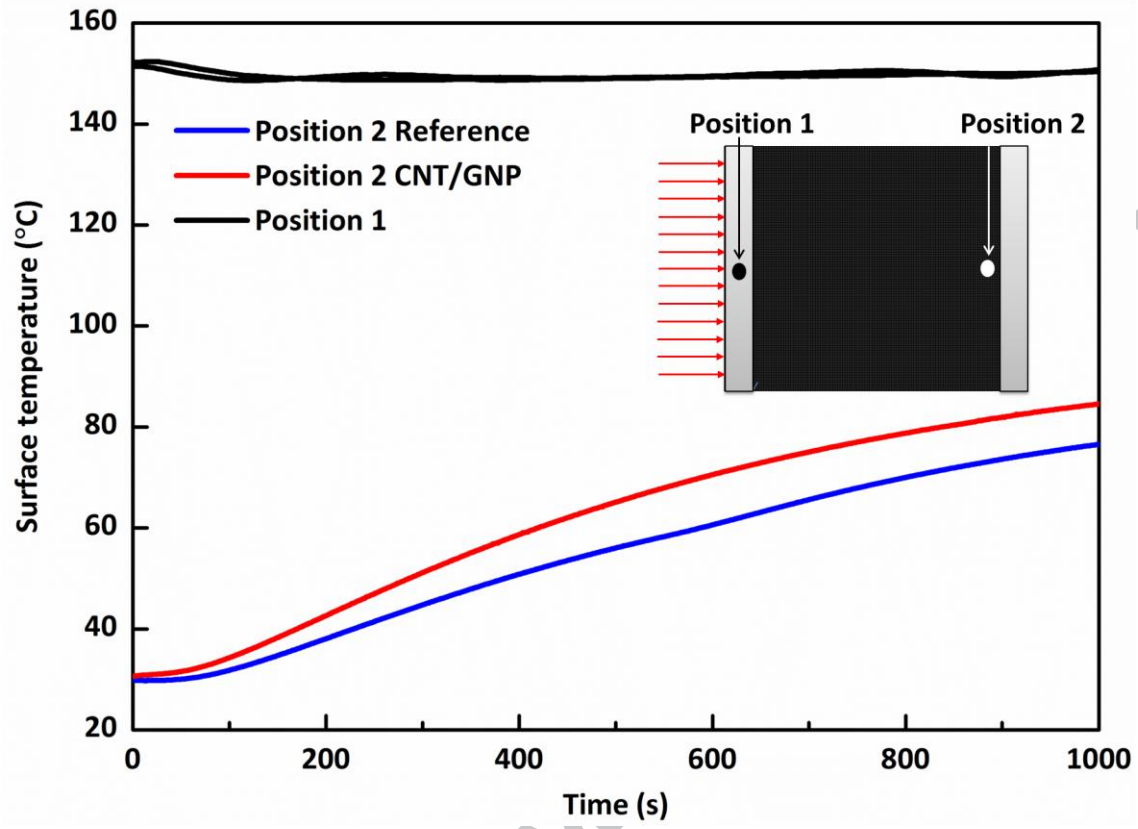

Fig. 5. Variations of temperature at position 2 for hybrid CNT/GNP spray coated panel and reference CFRP panel with the coating layer facing down (inset shows a schematic of the thermocouple positions).

Modelling of Heat Transfer through the Coating Layer

Fig.6 shows the physical model [56] of the heat transfer through the conductive nanocoating layer. The coating layer is facing upwards, hence its upper surface is in contact with air and its lower surface in contact with the CFRP laminate. *L*, *W* and *t* are the length, width and thickness of the coating layer, respectively. The left end of the panel surface was firmly attached to a strip with a constant temperature while the surface temperature T_0 (position 1) was measured by a thermocouple. The heat is assumed to transfer through the coating layer in the *x*-direction by conduction (one dimensional) and transfer to the surrounding air by convection and radiation since the surface temperature T_0 is higher than the air temperature T_a and that of surfaces of the test room. Since the thickness *t* of the layer is much smaller than its length and width, the convective heat transfer from the side and right end areas of the layer is negligible.

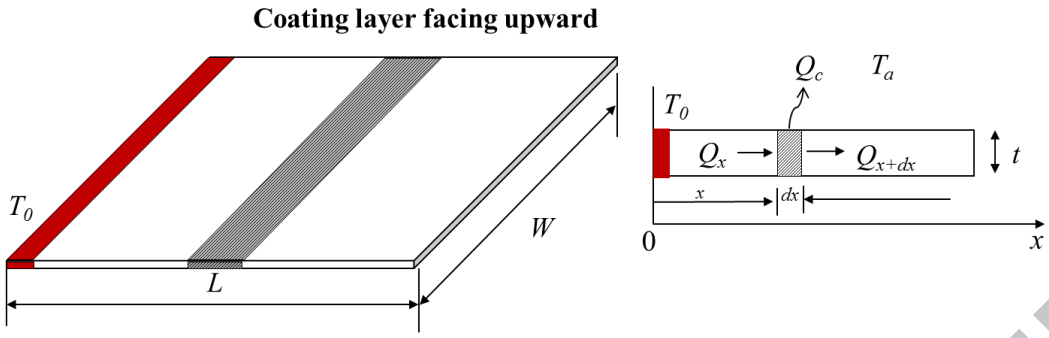

Fig. 6. Physical model of heat transfer through a coating layer (coating layer facing upward).

The cross-sectional area for heat conduction is $A = Wt$, the perimeter for heat convection is $P = W$. Taking a small element with length dx, the heat transfer by conduction into the element is Q_x,

$$Q_x = -\lambda A \frac{dT}{dx} \qquad \text{Equation (2)}$$

where λ is the thermal conductivity of the coating layer. The heat transfer by conduction of the element is Q_{x+dx},

$$Q_{x+dx} = Q_x + \frac{dQ_x}{dx} dx \qquad \text{Equation (3)}$$

The heat transfer by convection from the upper surface of the layer to air is Q_c.

$$Q_c = aPdx(T - T_a) \qquad \text{Equation (4)}$$

where α is the heat-transfer coefficient, T is the temperature of the layer at x. Considering steady state, one dimensional heat conduction, and using heat balance Equations (2-4), we obtain

$$\frac{d^2T}{dx^2} - \frac{aP}{\lambda A}(T - T_a) = 0 \qquad \text{Equation (5)}$$

The boundary conditions are

$$T = T_0 \quad at \quad x = 0 \qquad \text{Equation (6)}$$

$$\frac{dT}{dx} = 0 \quad at \quad x = L \qquad \text{Equation (7)}$$

The solution of Equation (5) with subject to the boundary conditions (6-7) gives the temperature distribution in the layer along the x-direction as

$$T - T_a = \frac{(T_0 - T_a)\cosh[m(\mathrm{L} - x)]}{\cosh(\mathrm{mL})}$$ Equation (8)

Where $m = \sqrt{\alpha P / \lambda A}$. The convective heat-transfer coefficient α can be estimated using an empirical correlation available for natural convective heat transfer of air from a hot horizontal flat surface facing upward [56].

$$Nu = 0.54 Ra^{1/4}$$ Equation (9)

where $Nu = \frac{\alpha L}{\lambda_a}$ and $Ra = \frac{g C_{Pa} \mu_a \beta_a (T - T_a) W^3}{\lambda_a \, v_a^{\,2}}$ are Nusselt number and Rayleigh number, respectively, λ_a is the thermal conductivity of air, g is the specific force of gravity, C_{pa} is the specific heat capacity of air at constant pressure, μ_a is dynamic viscosity of air, β_a is volume coefficient of expansion of air, v_a is the kinematic viscosity of air. Equation (9) is valid in the range of $2.6\times10^4 \leq R_a \leq 10^7$.

The properties of air at atmospheric pressure and room temperature (about 300 K) can be found in [56]: C_{pa} = 1.0 kJ/kg K; μ_a = 1.846×10^{-5} kg/m s; v_a = 15.69×10^{-6} m^2/s; λ_a = 0.026 W/m K; β_a = 3.3×10^{-3}/k. The dimensions of the test panel are L = 0.07m, W = 0.05m, t = 5×10^{-6} m. Under these conditions, we find Ra = 8.16×10^5, $N_u = 30.06$, α = 11.16 W/m^2 K. The estimated heat-transfer coefficient is in the range of such a case. Therefore m is calculated to be $15000\lambda^{-0.5}$.

Fig. 7a-d show experimental results on specimens coherent with the physical model in **Fig. 6,** but now with the coating layer facing upward to allow the recording of thermal images. In this case thermal images of the whole upper panel surface are continuously recorded by an infrared camera. The surface temperature distributions, of the CNT/GNP hybrid coated panel, are shown at four different time intervals. At τ = 0 s the surface temperature of the panel (black colour) is uniform at a room temperature of about 25 °C (**Fig. 7a)**. At τ = 60 s the surface temperature varies rapidly from left to right over two thirds of the panel length (**Fig. 7b**). As the surface temperature of the panel increases, heat is transferred along the length by conduction and also to the surrounding air by convection and radiation. At τ = 100 s the surface temperature variation reaches the right end of the panel (**Fig. 7c)**. At τ = 1000 s the surface temperature profile reaches a

steady state (**Fig. 7d**). The surface temperature distribution follows an exponential function along the *x*-direction. It is also noted that the surface temperature variation in the width direction is fairly uniform in all cases, indicating good localisation and dispersion of the hybrid nanofillers as well as one-dimensional heat transfer in the *x*-direction. The steady state surface temperature profile is shown in **Fig. 7e.** Surface temperatures at several locations were measured and plotted against *x***.** Note that at each location several temperatures along the width direction were measured and their average value was taken as the temperature at this location. The temperature variation in the width direction is shown by the error bar.

A physical model of the heat transfer through the coating layer is proposed and the analytical results can be used to interpret the temperature profile in **Fig. 7e.** The temperature *T* in the layer along the *x*-direction can be described by Equation (8). The main uncertainties involved in the measurements and calculations include: (1) in **Fig. 7**, the temperature measured using thermocouples due to contact thermal resistance between the thermocouple lead and the surface of the coating layer; (2) the thermal conductivity of the coating layer consisting of CNTs, GNPs and epoxy; (3) the radiation heat transfer rate estimated at about 15% of the total heat transfer. To calculate the temperature distribution in the coating layer along the *x*-direction, different values of thermal conductivity (λ) of the coating layer (100, 200, 800, 1000, 1500, 2000 $W \cdot m^{-1} \cdot K^{-1}$) were used in Equation (8) and compared with the experimental data. For example, when λ = 2000 $W \cdot m^{-1} \cdot K^{-1}$, the temperature distribution in the coating layer along the x-direction can be expressed as $T = T_a + 0.364(T_0 - T_a)\cosh(1.67 - 33.4x)$.

It can be seen from **Fig. 7e** that the measured surface temperature profiles are generally in good agreement with those predicted by Equation (8). The CNT/GNP hybrid coated panel can be fitted assuming a thermal conductivity of 1500 $W \cdot m^{-1} \cdot K^{-1}$, while the reference panel can be fitted by a thermal conductivity of 200 $W \cdot m^{-1} \cdot K^{-1}$. The analytical results show that the CNT/GNP hybrid nanoparticle coating provides a substantial increase in surface thermal conductivity, estimated to be more than 7 times higher than that of the reference panel. Thermal conductivities of Cu mesh and Al mesh are comparable at 400 $W \cdot m^{-1} \cdot K^{-1}$ and 200 $W \cdot m^{-1} \cdot K^{-1}$, respectively, highlighting the

potential of the proposed hybrid nanocoating system. Experimental results are also compared with representative data from literature in **Table 2**.

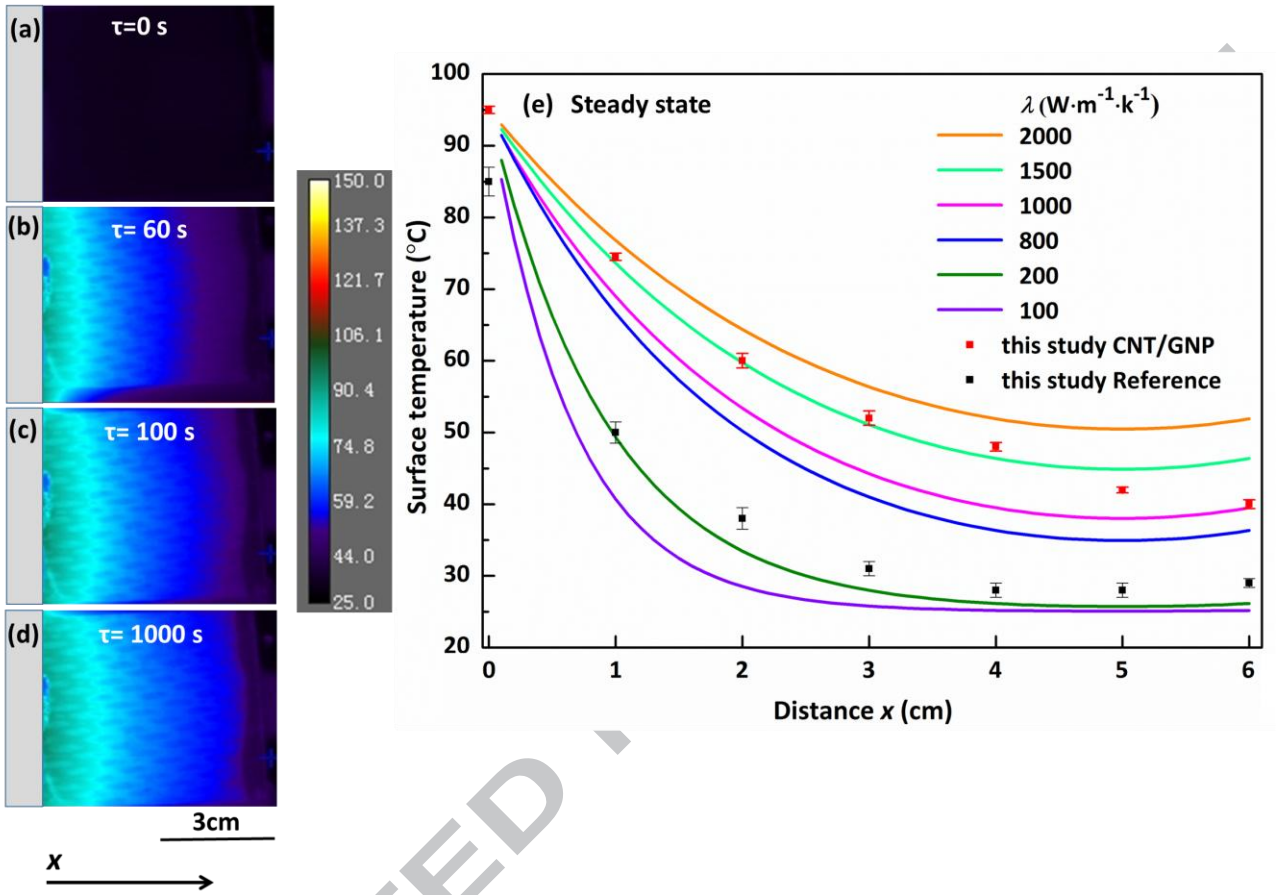

Fig. 7. (a-d) Thermal images of hybrid CNT/GNP coated CFRP captured by infrared camera; (e) comparison of the predicted and measured surface temperatures of hybrid CNT/GNP coated CFRP (in red) and CFRP reference panel (in black).

Table 2. Thermal conductivity of different coating materials.

Materials	*Thickness*	λ (W $m^{-1}K^{-1}$) 25° C	Refs
70 % diamond/Cu composites	0.40 mm	742	[57]
Stainless steel **mesh** with **Cu** micropillars	0.28 mm	1398	[58]
5 vol.% MWCNT/Cu	18.04 µm	404	[59]
10 vol.% MWCNT/Cu	12.20 µm	418	
20 vol.% MWCNT/Cu	4.80 µm	447	
30 vol.% MWCNT/Cu	2.30 µm	478	
Al mesh	0.30 mm	237	[60]
Cu mesh	0.25 mm	385	[61]
Monolayer graphene	0.34 nm	5000	[62]
SWCNT		3000	[63]
GNP/CNT	4.5-5.0 µm	1500	this study

4. CONCLUSIONS

A simple and versatile method to deposit and localize hybrid nanocarbons as a conductive coating onto a carbon fibre preform was demonstrated. Spray coating of hybridized CNT and GNP nanofillers lowered the surface electrical resistivity of laminates from 2-3 Ω/sq (for reference CFRP) to 1.03×10^{-3} Ω/sq (for CNT only coating) and 3.43×10^{-4} Ω/sq (for CNT/GNP hybrid coating), with the hybrid CNT/GNP system demonstrating certain levels of synergistic effects. The surface electrical resistivity of hybrid CNT/GNP coatings approaches that of commercial Cu mesh ($0.1\text{-}1.7\times10^{-4}$ Ω/sq) but at a fraction of the areal density (0.4 $g\cdot m^{-2}$ compared to 50-1000 $g\cdot m^{-2}$ for commercial metallic meshes). Thermal conductivity was increased from 200 $W\cdot m^{-1}\cdot K^{-1}$ (for reference CFRP) to 1500 $W\cdot m^{-1}\cdot K^{-1}$, for panels spray coated with CNT/GNP hybrids.

These extremely high specific electrical and thermal conductivity values make spray coated hybrid CNT/GNP nanocarbons a promising alternative to metal meshes for applications like LSP and EMI shielding of composite structures. Additional benefits reside in the versatility and scalability of the spraying process and the prevention of any galvanic corrosion caused by materials with different electro-chemical potentials.

ACKNOWLEDGEMENTS

This research has received funding from NanoSynth Project funded by the Technology Strategy Board (TSB) through the Technology Inspired Innovation – NANO Competition, No. 101257. Y.L. would also like to acknowledge the financial support through the China Scholarship Council (CSC) scheme.

COMPETING INTERESTS

The authors declare that there is no conflict of interest regarding the publication of this paper.

REFERENCES

[1] Soutis C. Carbon Fiber Reinforced Plastics in Aircraft Construction. Materials Science and Engineering: A. 2005;412(1):171-176.

[2] Zhang H, Liu Y, Kuwata M, Bilotti E, Peijs T. Improved Fracture Toughness and Integrated Damage Sensing Capability by Spray Coated Cnts on Carbon Fibre Prepreg. Composites Part A: Applied Science and Manufacturing. 2015;70(102-110.

[3] Suherman H, Sahari J, Sulong AB. Electrical Properties of Carbon Nanotubes-Based Epoxy Nanocomposites for High Electrical Conductive Plate. Advanced Materials Research: Trans Tech Publ; 2011. p. 559-564.

[4] Gardner G. Lightning Strike Protection for Composite Structures. High performance composites. 2006;14(4):44.

[5] Feraboli P, Miller M. Damage Resistance and Tolerance of Carbon/Epoxy Composite Coupons Subjected to Simulated Lightning Strike. Composites Part A: Applied Science and Manufacturing. 2009;40(6):954-967.

[6] Suzuki Y, Todoroki A, Matsuzaki R, Mizutani Y. Impact-Damage Visualization in Cfrp by Resistive Heating: Development of a New Detection Method for Indentations Caused by Impact Loads. Composites Part A: Applied Science and Manufacturing. 2012;43(1):53-64.

[7] Archambault G, Jodoin B, Gaydos S, Yandouzi M. Metallization of Carbon Fiber Reinforced Polymer Composite by Cold Spray and Lay-up Molding Processes. Surf. Coat. Technol. 2016;300(78-86.

[8] Welch JM. Repair Design, Test, and Process Considerations for Lightning Strikes. Joint FAA-Boeing-Airbus damage tolerance workshop, Amsterdam, The Netherlands2007.

[9] Zhang B, Patlolla VR, Chiao D, Kalla DK, Misak H, Asmatulu R. Galvanic Corrosion of Al/Cu Meshes with Carbon Fibers and Graphene and Ito-Based Nanocomposite Coatings as Alternative Approaches for Lightning Strikes. The International Journal of Advanced Manufacturing Technology. 2013;67(5-8):1317-1323.

[10] http://www.compositesworld.com/articles/lightning-strike-protection-strategies-for-composite-aircraft (accessed 23 August 2016)

[11] Davis GD, Vargo TG, Dalgleish AW, Deason D, Space UA, Command MD. Smart Appliqués for Corrosion Protection and Health Monitoring. Proc. 2003 Tri-Services Conference on Corrosion2003.

[12] Zhang P, Huang Y, Geubelle P, Klein P, Hwang K. The Elastic Modulus of Single-Wall Carbon Nanotubes: A Continuum Analysis Incorporating Interatomic Potentials. International Journal of Solids and Structures. 2002;39(13):3893-3906.

[13] Lee C, Wei X, Kysar JW, Hone J. Measurement of the Elastic Properties and Intrinsic Strength of Monolayer Graphene. science. 2008;321(5887):385-388.

[14] Stankovich S, Dikin DA, Dommett GH, Kohlhaas KM, Zimney EJ, Stach EA, Piner RD, Nguyen ST, Ruoff RS. Graphene-Based Composite Materials. nature. 2006;442(7100):282-286.

[15] Nika D, Ghosh S, Pokatilov E, Balandin A. Lattice Thermal Conductivity of Graphene Flakes: Comparison with Bulk Graphite. Applied Physics Letters. 2009;94(20):203103.

[16] Gagné M, Therriault D. Lightning Strike Protection of Composites. PrAeS. 2014;64(1-16.

[17] Wu H, Drzal LT. Graphene Nanoplatelet Paper as a Light-Weight Composite with Excellent Electrical and Thermal Conductivity and Good Gas Barrier Properties. Carbon. 2012;50(3):1135-1145.

[18] Levitsky IA, Euler WB, Karachevtsev VA. Photophysics of Carbon Nanotubes Interfaced with Organic and Inorganic Materials: Springer Science & Business Media; 2012.

[19] Morozov S, Novoselov K, Katsnelson M, Schedin F, Elias D, Jaszczak JA, Geim A. Giant Intrinsic Carrier Mobilities in Graphene and Its Bilayer. Physical review letters. 2008;100(1):016602.

[20] Al-Rub RKA, Ashour AI, Tyson BM. On the Aspect Ratio Effect of Multi-Walled Carbon Nanotube Reinforcements on the Mechanical Properties of Cementitious Nanocomposites. Construction and Building Materials. 2012;35(647-655.

[21] May P, Khan U, O'Neill A, Coleman JN. Approaching the Theoretical Limit for Reinforcing Polymers with Graphene. Journal of Materials Chemistry. 2012;22(4):1278-1282.

[22] Compton OC, Kim S, Pierre C, Torkelson JM, Nguyen ST. Crumpled Graphene Nanosheets as Highly Effective Barrier Property Enhancers. Advanced materials. 2010;22(42):4759-4763.

[23] Zhang H, Liu Y, Huo S, Briscoe J, Tu W, Picot OT, Rezai A, Bilotti E, Peijs T. Filtration Effects of Graphene Nanoplatelets in Resin Infusion Processes: Problems and Possible Solutions. Compos. Sci. Technol. 2017;139(138-145.

[24] Zhang S, Lin L, Deng H, Gao X, Bilotti E, Peijs T, Zhang Q, Fu Q. Dynamic Percolation in Highly Oriented Conductive Networks Formed with Different Carbon Nanofillers. Colloid. Polym. Sci. 2012;290(14):1393-1401.

[25] Bilotti E, Zhang H, Deng H, Zhang R, Fu Q, Peijs T. Controlling the Dynamic Percolation of Carbon Nanotube Based Conductive Polymer Composites by Addition of Secondary Nanofillers: The Effect on Electrical Conductivity and Tuneable Sensing Behaviour. Composites Science and Technology. 2013;74(85-90.

[26] Deng H, Skipa T, Bilotti E, Zhang R, Lellinger D, Mezzo L, Fu Q, Alig I, Peijs T. Preparation of High‐Performance Conductive Polymer Fibers through Morphological Control of Networks Formed by Nanofillers. Advanced Functional Materials. 2010;20(9):1424-1432.

[27] Deng H, Zhang R, Bilotti E, Loos J, Peijs T. Conductive Polymer Tape Containing Highly Oriented Carbon Nanofillers. Journal of applied polymer science. 2009;113(2):742-751.

[28] Hourston DJ, Lane JM, Macbeath NA. Toughening of Epoxy Resins with Thermoplastics. Ii. Tetrafunctional Epoxy Resin‐Polyetherimide Blends. Polymer international. 1991;26(1):17-21.

[29] Kotov NA. Materials Science: Carbon Sheet Solutions. Nature. 2006;442(7100):254-255.

[30] Wang Z, Liang Z, Wang B, Zhang C, Kramer L. Processing and Property Investigation of Single-Walled Carbon Nanotube (Swnt) Buckypaper/Epoxy Resin Matrix Nanocomposites. Composites Part A: Applied Science and Manufacturing. 2004;35(10):1225-1232.

[31] Gou J, Tang Y, Liang F, Zhao Z, Firsich D, Fielding J. Carbon Nanofiber Paper for Lightning Strike Protection of Composite Materials. Composites Part B: Engineering. 2010;41(2):192-198.

[32] Silva MJd, Sanches AO, Malmonge LF, Malmonge JA. Electrical, Mechanical, and Thermal Analysis of Natural Rubber/Polyaniline-Dbsa Composite. Materials Research. 2014;17(59-63.

[33] Kumar V, Yokozeki T, Goto T, Takahashi T. Mechanical and Electrical Properties of Pani-Based Conductive Thermosetting Composites. Journal of Reinforced Plastics and Composites. 2015;34(16):1298-1305.

[34] Hirano Y, Yokozeki T, Ishida Y, Goto T, Takahashi T, Qian D, Ito S, Ogasawara T, Ishibashi M. Lightning Damage Suppression in a Carbon Fiber-Reinforced Polymer with a Polyaniline-Based Conductive Thermoset Matrix. Composites Science and Technology. 2016;127(1-7.

[35] Lu J, Moon K-S, Kim B-K, Wong C. High Dielectric Constant Polyaniline/Epoxy Composites Via in Situ Polymerization for Embedded Capacitor Applications. Polymer. 2007;48(6):1510-1516.

[36] Del Castillo-Castro T, Castillo-Ortega M, Herrera-Franco P. Electrical, Mechanical and Piezo-Resistive Behavior of a Polyaniline/Poly (N-Butyl Methacrylate) Composite. Composites Part A: Applied Science and Manufacturing. 2009;40(10):1573-1579.

[37] Katunin A, Krukiewicz K, Turczyn R, Sul P, Łasica A, Bilewicz M. Synthesis and Characterization of the Electrically Conductive Polymeric Composite for Lightning Strike Protection of Aircraft Structures. Composite Structures. 2017;159(773-783.

[38] Yokozeki T, Goto T, Takahashi T, Qian D, Itou S, Hirano Y, Ishida Y, Ishibashi M, Ogasawara T. Development and Characterization of Cfrp Using a Polyaniline-Based Conductive Thermoset Matrix. Composites Science and Technology. 2015;117(277-281.

[39] Zhang H, Kuwata M, Bilotti E, Peijs T. Integrated Damage Sensing in Fibre-Reinforced Composites with Extremely Low Carbon Nanotube Loadings. J. Nanomater. 2015;2015(Article ID 785834):7.

[40] Zhang H, Bilotti E, Peijs T. Nano-Engineered Hierarchical Carbon Fibres and Their Composites: Preparation, Properties and Multifunctionalities. In: Beaumont PWR, Soutis C, Hodzic A, editors. The Structural Integrity of Carbon Fiber Composites: Fifty Years of Progress and Achievement of the Science, Development, and Applications. Cham: Springer International Publishing; 2017. p. 101-116.

[41] Zhang. H, Liu. Y, Bilotti. E, Peijs. T. In-Situ Monitoring of Interlaminar Shear Damage in Carbon Fibre Composites. Advanced Composite Letters. 2015;24, 4(04):92-97.

[42] Chakravarthi DK, Khabashesku VN, Vaidyanathan R, Blaine J, Yarlagadda S, Roseman D, Zeng Q, Barrera EV. Carbon Fiber‐Bismaleimide Composites Filled with Nickel‐Coated Single‐Walled Carbon Nanotubes for Lightning‐Strike Protection. Advanced Functional Materials. 2011;21(13):2527-2533.

[43] Shin MK, Lee B, Kim SH, Lee JA, Spinks GM, Gambhir S, Wallace GG, Kozlov ME, Baughman RH, Kim SJ. Synergistic Toughening of Composite Fibres by Self-Alignment of Reduced Graphene Oxide and Carbon Nanotubes. Nature communications. 2012;3(650.

[44] Yang S-Y, Lin W-N, Huang Y-L, Tien H-W, Wang J-Y, Ma C-CM, Li S-M, Wang Y-S. Synergetic Effects of Graphene Platelets and Carbon Nanotubes on the Mechanical and Thermal Properties of Epoxy Composites. Carbon. 2011;49(3):793-803.

[45] Li Y, Zhang, H., Peijs, T., & Bilotti, E. Graphene Delivery Systems for Hierarchical Fiber Reinforced Composites. MRS Advances. 2016;1(19):1339-1344.

[46] Zhang H, Bharti A, Li Z, Du S, Bilotti E, Peijs T. Localized Toughening of Carbon/Epoxy Laminates Using Dissolvable Thermoplastic Interleaves and Electrospun Fibres. Composites Part A: Applied Science and Manufacturing. 2015;79(116-126.

[47] Wong DWY, Zhang H, Bilotti E, Peijs T. Interlaminar Toughening of Woven Fabric Carbon/Epoxy Composite Laminates Using Hybrid Aramid/Phenoxy Interleaves. Composites Part A: Applied Science and Manufacturing. 2017;101(Supplement C):151-159.

[48] Li Y, Zhang H, Crespo M, Porwal H, Picot O, Santagiuliana G, Huang Z, Barbieri E, Pugno NM, Peijs T. In Situ Exfoliation of Graphene in Epoxy Resins: A Facile Strategy to Efficient and Large Scale Graphene Nanocomposites. ACS Applied Materials & Interfaces. 2016;8(36):24112-24122.

[49] ASTM D4496-87(1998e1, Standard Test Method for D-C Resistance or Conductance of Moderately Conductive Materials, ASTM International, West Conshohocken, PA, 1998, www.astm.org).

[50] Yu J, Choi HK, Kim HS, Kim SY. Synergistic Effect of Hybrid Graphene Nanoplatelet and Multi-Walled Carbon Nanotube Fillers on the Thermal Conductivity of Polymer Composites and Theoretical Modeling of the Synergistic Effect. Composites Part A: Applied Science and Manufacturing. 2016;88(79-85.

[51] Cheng Y, Lu S, Zhang H, Varanasi CV, Liu J. Synergistic Effects from Graphene and Carbon Nanotubes Enable Flexible and Robust Electrodes for High-Performance Supercapacitors. Nano letters. 2012;12(8):4206-4211.

[52] Zhou T, Wang X, Cheng P, Wang T, Xiong D. Improving the Thermal Conductivity of Epoxy Resin by the Addition of a Mixture of Graphite Nanoplatelets and Silicon Carbide Microparticles. Express Polymer Letters. 2013;7(7):

[53] Chu H, Zhang Z, Liu Y, Leng J. Self-Response Multi-Functional Composite Material Base on Carbon Nanotube Paper Using Deicing, Flame Retardancy, Thermal Insulation, and Lightning-Strike Protection. SPIE Smart Structures and Materials+ Nondestructive Evaluation and Health Monitoring: International Society for Optics and Photonics; 2015. p. 94320S-94320S-94328.

[54] http://www.astrosealproducts.com/properties.html (accessed 12 May 2016)

[55] Vishnyakov L, Pereselentseva L, Vishnyakova E. Knitted Soldered Meshes and Nanostructured Carbon Particles for Lightning Protection of Composite Wind Turbine Blades. Powder Metall. Met. Ceram. 2014;53(5-6):368-374.

[56] Holman J. Heat Transfer, Eighth Si Metric Edition. McGraw-Hill Inc; 2001.

[57] Yoshida K, Morigami H. Thermal Properties of Diamond/Copper Composite Material. Microelectronics Reliability. 2004;44(2):303-308.

[58] Xu S, Lewis RJ, Liew L-A, Lee Y-C, Yang R. Development of Ultra-Thin Thermal Ground Planes by Using Stainless-Steel Mesh as Wicking Structure. Journal of Microelectromechanical Systems. 2016;25(5):842-844.

[59] Zheng X, Park CW. Experimental Study of the Sintered Multi-Walled Carbon Nanotube/Copper Microstructures for Boiling Heat Transfer. Applied Thermal Engineering. 2015;86(14-26.

[60] Hatch JE, Association A. Aluminum: Properties and Physical Metallurgy: ASM International; 1984.

[61] Tian J, Kim T, Lu T, Hodson H, Queheillalt D, Sypeck D, Wadley H. The Effects of Topology Upon Fluid-Flow and Heat-Transfer within Cellular Copper Structures. International Journal of Heat and Mass Transfer. 2004;47(14):3171-3186.

[62] Geim AK. Graphene: Status and Prospects. science. 2009;324(5934):1530-1534.

[63] Balandin AA. Thermal Properties of Graphene and Nanostructured Carbon Materials. Nature materials. 2011;10(8):569-581.